CrossMark

ORIGINAL PAPER

# Depositional modes and lake-level variability at Lake Towuti, Indonesia, during the past ~29 kyr BP

Hendrik Vogel · James M. Russell · Sri Yudawati Cahyarini · Satria Bijaksana · Nigel Wattrus · Janet Rethemeyer · Martin Melles

**Abstract** Lake Towuti (2.5°S, 121.5°E) is a long-lived, tectonic lake located on the Island of Sulawesi, Indonesia, and in the center of the Indo-Pacific warm pool (IPWP). Lake Towuti is connected with upstream lakes Matano and Mahalona through the Mahalona River, which constitutes the largest inlet to the lake. The Mahalona River Delta is prograding into Lake Towuti's deep northern basin thus exerting significant control on depositional processes in the basin. We combine high-resolution seismic reflection and sedimentological datasets from a 19.8-m-long sediment piston core from the distal edge of this delta to characterize fluctuations in deltaic sedimentation during the past ~29 kyr BP and their relation to climatic change. Our datasets reveal that, in the present, sedimentation is strongly influenced by deposition of laterally transported sediments sourced from the Mahalona River Delta. Variations in the amount of laterally transported sediments, as expressed by coarse fraction amounts in pelagic muds and turbidite recurrence rates and cumulative thicknesses, are primarily a function of lake-level induced delta slope instability and delta progradation into the basin. We infer lowest lake-levels between ~29 and 16, a gradual lake level rise between ~16 and 11, and high lake-levels between ~11 and 0 kyr BP. Periods of highest turbidite deposition, ~26 to 24 and ~18 to

H. Vogel (✉)
Institute of Geological Sciences & Oeschger Centre for Climate Change Research, University of Bern, Baltzerstr. 1+3, 3012 Bern, Switzerland
e-mail: hendrik.vogel@geo.unibe.ch

J. M. Russell
Department of Earth, Environmental, and Planetary Sciences, Brown University, Box 1846, Providence, RI 02912, USA
e-mail: James_Russell@brown.edu

S. Y. Cahyarini
Research Centre for Geotechnology, Indonesian Institute of Sciences (LIPI), Bandung, Indonesia
e-mail: yudawati@yahoo.com

S. Bijaksana
Faculty of Mining and Petroleum Engineering, Institut Teknologi Bandung, Jalan Ganesa 10, Bandung, Indonesia
e-mail: satria@fi.itb.ac.id

N. Wattrus
Large Lakes Observatory, University of Minnesota Duluth, 10 University Drive, Duluth, MN 55812, USA
e-mail: nwattrus@d.umn.edu

J. Rethemeyer · M. Melles
Institute of Geology and Mineralogy, University of Cologne, Zülpicher Straße 49a, 50674 Cologne, Germany
e-mail: janet.rethemeyer@uni-koeln.de

M. Melles
e-mail: mmelles@uni-koeln.de

16 kyr BP coincide with Heinrich events 2 and 1, respectively. Our lake-level reconstruction therefore supports previous observations based on geochemical hydroclimate proxies of a very dry last glacial and a wet Holocene in the region, and provides new evidence of millennial-scale variations in moisture balance in the IPWP.

**Keywords** Hydroclimate · Lake Towuti · Indonesia · Lake-level · Depositional processes · Indo-Pacific warm pool

## Introduction

Three large areas of deep atmospheric convection in the tropics [tropical Africa, Amazon basin, Indo-Pacific warm pool (IPWP)] function as important drivers of atmospheric circulation and exert a strong control on heat and water vapor transfer from the tropics into higher latitudes on Earth. Variability in the magnitude of deep atmospheric convection in the largest of these areas, the IPWP, is thought to be an important component in the initiation and amplification of global climatic change on orbital to millennial time scales (Cane and Clement 1999; Pierrehumbert 1999; Clement et al. 2001; Chiang 2009). In order to better understand the impact of IPWP variability on global climate changes, long and highly resolved paleoclimate records, from sites suitable to record changes in convective energy in the IPWP region, are required.

Lake Towuti is a long-lived (Rintelen et al. 2012) tectonic lake (Van Bemmelen 1970) located on the Island of Sulawesi, Indonesia, in the centre of the IPWP. Its location and longevity make it an important site to study long-term paleoclimate change in this understudied region of our planet (Russell and Bijaksana 2012). The value of the climatic signal preserved in Towuti's sediments has recently been highlighted in a study that focused on hydroclimatic changes during the past 60 kyr BP (Russell et al. 2014). Russell et al. (2014) applied titanium (Ti) as elemental tracer for terrestrial runoff and the carbon isotopic composition of terrestrial plant leaf waxes ($\delta^{13}C_{wax}$) as indicator for moisture-balance-driven changes in vegetation surrounding Lake Towuti. The coherent signal produced by these datasets implies that the region experienced

significant changes in moisture availability, with interstadial/interglacial periods of marine isotope stage 3 (MIS 3) and the Holocene being characterized by wetter and stadial/glacial periods of MIS 4 and 2 being characterized by substantially drier conditions (Russell et al. 2014). These changes in moisture availability have also influenced lake water oxygenation and catchment processes at Lake Towuti (Costa et al. 2015; Tamuntuan et al. 2015), with deeper mixing and a well oxygenated water column as a result of enhanced evaporative surface water cooling during dry periods of MIS 4 and 2. While these datasets show a coherent pattern of hydroclimatic change associated with glacial/interglacial periods (Russell et al. 2014), a dataset suitable to trace changes in lake-level driven depositional processes is still missing from Lake Towuti. A record of the timing and magnitude of lake-level change may allow a more quantitative reconstruction of changes in moisture availability from Lake Towuti.

Lake-level changes in lacustrine settings are commonly inferred from the identification and direct and/or indirect dating of subaerial and subaquatic terrace levels (Scholz et al. 2007; Anselmetti et al. 2009; Lindhorst et al. 2010). More qualitative approaches have utilized geochemical (Haberzettl et al. 2005) or biological indicators (Gasse et al. 1989; Alin and Cohen 2003). Changes in water-level also exert a strong control on slope stability and river delta dynamics in lacustrine (Anselmetti et al. 2009; Moernaut et al. 2010) and marine settings (Einsele 1996; Muto and Steel 2002; Lee 2009) affecting sediment physical properties. Therefore, the identification of temporal changes in sediment physical properties that are controlled by lake-level fluctuations offers another possibility to trace back changes in lake-level over time. Here we utilize seismic reflection data in combination with lithological and sedimentological information from sediment piston cores from Lake Towuti's deep northern basin (Figs. 1, 2) in order to: (1) identify the depositional processes controlling sedimentation during the past ∼29 kyr BP; (2) recognize the influence of changes in moisture balance variations on these depositional processes, (3) distinguish lithological and sedimentological indicators suitable to trace changes in sediment deposition related to climatically induced lake-level variations; and (4) reconstruct relative lake-level variability at Lake Towuti's during the past ∼29 kyr BP.
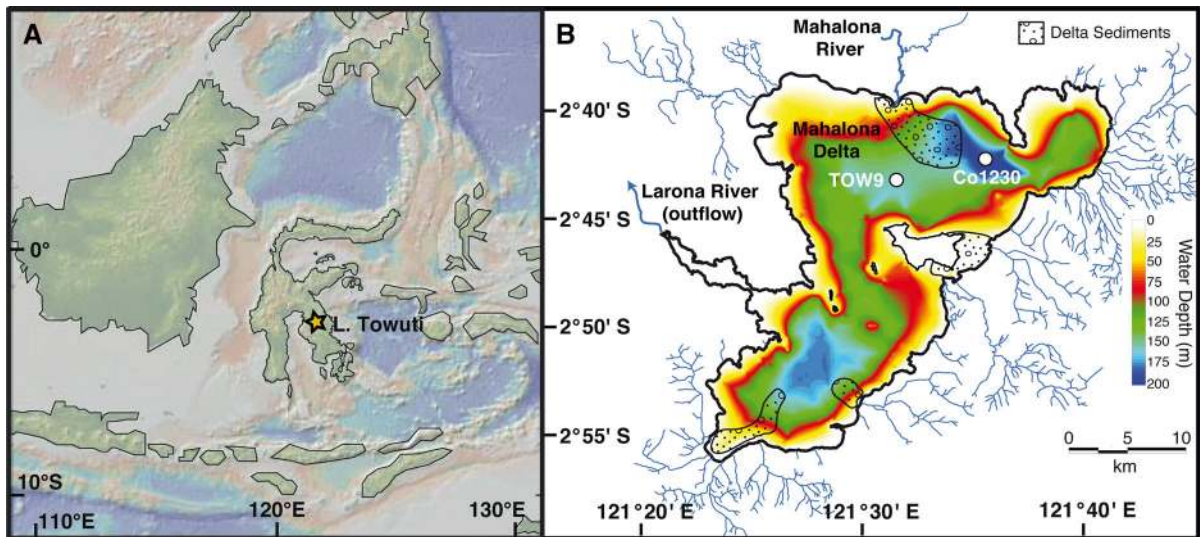
**Fig. 1 A** Map of the maritime continent. The *star* marks the location of Lake Towuti on the Island of Sulawesi, Indonesia and **B** bathymetric map of Lake Towuti showing piston coring sites Co1230 and TOW9 as well as major tributaries and coarse-grained delta sediments. Bathymetry data was generated from CHIRP data. The spatial extend of the indicated coarse-grained delta sediments is based upon interpolating the boundaries between acoustically stratified sediments and those with low penetration

Study site

Lake Towuti (2°45′S, 121°30′E; 318 m a.s.l.; Fig. 1) is the largest lake (560 km$^2$, 203 m water depth) within the Malili Lake System, a chain of five tectonic lakes in Central Sulawesi, Indonesia. The three largest of these lakes, Matano, Mahalona, and Towuti are connected with surface outflow from Matano to Mahalona to Towuti, which drains into the Bay of Bone via the Larona River. Annual average air temperature at the lakeshore is 25.7 °C, with less than 1 °C variation in monthly mean temperatures. Precipitation averages 2540 mm year$^{-1}$ and is strongly controlled by the annual passage of the Intertropical Convergence Zone (ITCZ) and the Austral–Indonesian Summer Monsoon (AISM), with monthly maxima and minima in precipitation during April and August, respectively. El Niño events result in severe droughts and lake level reductions at Towuti, highlighted by a 3.5-m-decline and transition to closed-basin status during the 1997–1998 El Niño event (Tauhid and Arifian 2000).

The Island of Sulawesi is located within a complex tectonic setting characterized by convergence of the Eurasian, Indo-Australian, Caroline and Philippine Sea plates (Hamilton 1979; Hall 1996; Spakman and Hall 2010). This is also documented in the frequency of earthquakes with magnitude >5 earthquakes occurring on average every year on Sulawesi and in the vicinity of Lake Towuti (USGS earthquake density map; earthquake.usgs.gov/earthquakes/world/indonesia/density.php). Ultramafic bedrock of the East Sulawesi Ophiolite (Kadarusman et al. 2004) that is intensely weathered to thick lateritic horizons (Golightly and Arancibia 1979) occupies the majority of Lake Towuti's catchment.

Lake Towuti is relatively dilute (210 µS cm$^{-1}$), ultraoligotrophic, and circumneutral (pH ∼ 7.8) (Haffner et al. 2001; Lehmusluoto et al. 1995). The water column of Lake Towuti is weakly thermally stratified, but is known to mix at least occasionally (Costa et al. 2015). Lake Towuti is presently hydrologically open with outflow to the southwest into the Bay of Bone through the Larona River. Contemporary Lake Towuti has a balanced hydrological budget with inputs equaling losses at ∼8.8 m year$^{-1}$. By far the largest single input to Lake Towuti, accounting for ∼24 % of riverine water input, is from the Mahalona River, which drains the extensive catchments of Lake Matano and Mahalona to the north and forms a large delta that is actively prograding into the deep northern basin of the lake (Fig. 1). Direct precipitation on the
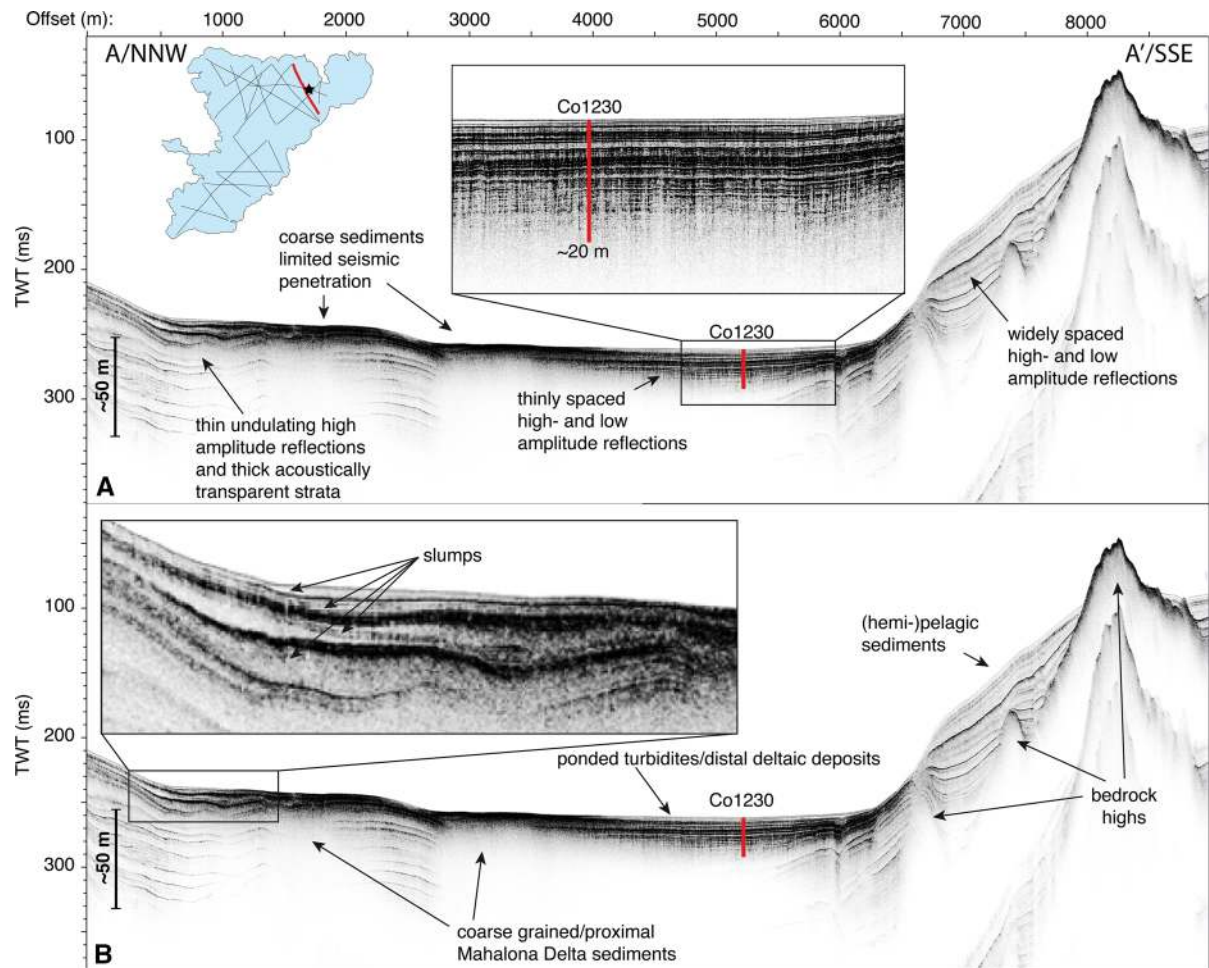
**Fig. 2** High-resolution seismic (3.5 kHz CHIRP) profile crossing Lake Towuti's deep northern basin from NNW to SSE (see *inset map* for location; *star* marks piston coring site Co1230). **A** Blow-up of sediment architecture around piston coring site Co1230 showing horizontal continuous and acoustically laminated high and low amplitude reflections and **B** blow-up showing mass wasting deposits/slumps originating from Mahalona Delta slopes. Hence, the seismic profile cuts through the slump deposits laterally

lake surface (~30 %) and rivers (~46 %) draining the direct catchment of the lake complete the hydrological inputs. Net evaporation from the lake surface (~15 %) and outflow through the Larona River (~85 %) constitute the main hydrological losses.

## Materials and methods

### Seismic survey

In August 2007 we collected ~250-km of high-resolution seismic reflection (CHIRP) data using an Edgetech[TM] 3200 high-penetration sub-bottom profiling system with an SB-424 towfish deployed from a local vessel (see inset in Fig. 2). Data were acquired using a 46-µs sampling interval, a 3–15 kHz swept frequency, and a 1-s shot rate corresponding to a ~1.74 m shot spacing. With some modifications, data were collected along tracklines generally oriented from WNW to ESE and SW to NE across the basin, roughly parallel and perpendicular to (respectively) the major faults in the region. The spacing between tracklines averages ~5 km. Positions of the ship were recorded using a Furano[TM] global positioning system. These seismic datasets were used for piston coring site

selection and characterization of depositional settings and sediment architecture in Lake Towuti.

### Sediment piston coring

Piston coring site Co1230 is located at 203 m water depth, in the northern basin and deepest part of Lake Towuti (2°42′19″S, 121°35′33″E; Figs. 1, 2). The site is located in a distal position to the Mahalona River Delta thereby avoiding coarse-grained deltaic deposits and erosional discordances from mass wasting processes (Figs. 1, 2). Core Co1230 was collected from a floating platform using an UWITEC percussion piston coring system equipped with a wire guided coring tool reentry system in July 2010. The floating platform was anchored on location during the entire 10 days it required to complete coring. In order to collect a complete sediment succession, consisting of individual 2-m-long core sections, we cored three overlapping holes down to 6, 16, and 20 m, respectively. Core loss between individual sections was minimal and a composite sequence of 19.8-m-length was composed after core splitting based on lithological features.

### Sediment analyses

Relative intensities for Iron (Fe), Titanium (Ti), Calcium (Ca), and Silicon (Si) were measured on core halves using an X-ray fluorescence (XRF) core scanner (ITRAX, Cox Ltd., Sweden), equipped with a Cr-tube set to 30 kV and 30 mA. Measurements were performed at 1-cm resolution using an integration time of 10-s per measurement. Magnetic susceptibility (MS) and color spectrophotometric measurements were conducted on core halves at 1 cm resolution using a Geotek Multisensor Core Logger (MSCL). The MSCL was equipped with a Bartington MS2E point sensor for MS measurements and a Konica Minolta color spectrophotometer for reflectance measurements between 360 and 740 nm. Spectrophotometer data were used to generate a synthetic color image for core Co1230. The lithogenic fractions of the samples were analyzed for particle size distribution after removal of organic matter ($H_2O_2$ 10 %) and authigenic minerals such as siderite (HCl 10 %). NaOH treatment was not applied due to the rarity of diatoms (<0.5 %), and because of high amounts of serpentine, which dissolves upon treatment with NaOH. Samples were treated with a dispersing agent

solution containing $Na_6P_6O_{18}$ and $Na_2CO_3$ prior to analysis using laser diffraction (Malvern Mastersizer 2000S).

### Radiocarbon dating and age-model

Radiocarbon dating was performed on 12 bulk organic carbon samples (Table 1) at the University of Cologne AMS facilities using standard protocols (Rethemeyer et al. 2013). We applied a reservoir correction established for the respective time interval for core TOW9 (Russell et al. 2014; Fig. 1), using paired macrofossil and bulk organic carbon samples, to all core Co1230 samples prior to calibration using the IntCal13.14C northern hemisphere terrestrial calibration curve (Reimer et al. 2013). The age-depth model for core Co1230 was calculated after omitting event deposits using the Clam software package and a smooth-spline function with a smoothing factor of 0.3 (Blaauw 2010). For the calculation of an age-depth model including event deposits and sedimentation rates resulting thereof, constant ages were assigned for each individual event deposit.

## Results

### Sediment architecture in Lake Towuti's deep northern sub-basin

Profile A–A′ (Fig. 2) shows a high-resolution CHIRP seismic line crossing the 203-m-deep northern basin from the Mahalona River Delta slopes in the NNW to bedrock highs in the SSE with coring site Co1230 in the central/deepest part of the basin. The CHIRP data indicates a very flat basin floor morphology that is fault bounded, with ∼60 to 100 m of imaged sediment. Sediments at coring site Co1230 appear acoustically laminated and consist of thinly spaced high amplitude reflections (Fig. 2A). Reflections show constant thicknesses on the decimeter scale and are characterized by horizontal continuity of individual reflections over several kilometers. Sediments deposited in the central basin pinch out towards the S and E where they grade into sediments characterized by more widely spaced high and low amplitude reflections that are draped onto slopes of bedrock highs bordering the basin (Fig. 2). Acoustic penetration is hampered towards the NNW, likely as a result of

**Table 1** Reservoir-corrected (according to Russell et al. 2014) and calibrated radiocarbon ages used for the age-depth model of core Co1230

| Sample ID | Depth (cm) | 14C age (years BP) | 1-sigma error (±) | Reservoir correction (14C years) | Reservoir corrected 14C age | Calibrated age (cal years BP) | 2-sigma error (±) | Material |
|---|---|---|---|---|---|---|---|---|
| S00465 | 160 | 3763 | 33 | 500 | 3263 | 3505 | 63 | Bulk OC |
| S00464 | 285 | 5136 | 34 | 500 | 4636 | 5405.5 | 59.5 | Bulk OC |
| S00463 | 402 | 6846 | 38 | 500 | 6346 | 7252.5 | 79.5 | Bulk OC |
| S00461 | 507 | 8456 | 41 | 500 | 7956 | 8838.5 | 147.5 | Bulk OC |
| S00459 | 664 | 11,926 | 52 | 1000 | 10,926 | 12,813.5 | 111.5 | Bulk OC |
| S00458 | 709 | 12,921 | 55 | 1000 | 11,921 | 13,714.5 | 146.5 | Bulk OC |
| S00457 | 1061 | 14,487 | 64 | 1000 | 13,487 | 16,254.5 | 230.5 | Bulk OC |
| S00455 | 1229 | 15,954 | 69 | 1000 | 14,954 | 18,164.5 | 202.5 | Bulk OC |
| S00555 | 1463 | 18,896 | 134 | 1000 | 17,896 | 21,661 | 383 | Bulk OC |
| S00554 | 1541 | 20,102 | 138 | 1000 | 19,102 | 23,025.5 | 396.5 | Bulk OC |
| S00553 | 1632 | 20,798 | 146 | 1000 | 19,798 | 23,832 | 361 | Bulk OC |
| S00552 | 1870 | 23,962 | 211 | 1000 | 22,962 | 27,225.5 | 428.5 | Bulk OC |

*Bulk OC* bulk organic carbon

abundance of coarser sediments in close proximity of the Mahalona River Delta. We mapped the contact between acoustically stratified sediments and those with low penetration in order to decipher the spatial extent of Mahalona Delta sediments in the northern basin (Fig. 1). The spatial extend of these sediments implies that the delta is primarily prograding into Lake Towuti's fault-bounded deep northern basin. Sediments deposited on the toe of the Mahalona River Delta exhibit more chaotic acoustic features characterized by thin undulating high amplitude reflections and thick acoustically transparent strata that are traced back to subaquatic slumping (Fig. 2B).

Lithology and geochemistry of core Co1230

Core Co1230 includes the uppermost 19.8 m of the horizontally bedded sediments in Lake Towuti's northern basin (Figs. 2, 3). Sediments in core Co1230 exhibit two distinctly different lithologies based upon their grain-size, color, and structural features (Figs. 3, 4). Lithotype 1 can, due to sharp basal and upper contacts, easily be distinguished from Lithotype 2 sediments. Lithotype 1 deposits are light brown to red–brown in color, occur throughout the entire Co1230 sediment sequence, and vary in thickness between 54 and 2 cm. Deposits occur either as individual beds interspersed with Lithotype 2 sediments or as successive beds without interspersed

Lithotype 2 deposits. Lithotype 1 beds typically show a sharp but generally non-erosive basal contact and normal gradation from middle-sand to clayey-silt with the gradation fading out into a more homogenous/massive clayey-sandy silt (Fig. 4). The coarse-grained basal parts of thicker Lithotype 1 deposits exhibit visible vertical variation in grain size. Individual sand-sized grains are angular to sub-angular in shape. The mineralogy of the sand-sized fraction is dominated by serpentine (>80 %) with minor amounts of quartz, Cr-spinell, pyroxene, chromite, and magnetite. The topmost part of Lithotype 1, in deposits with thicknesses >20 cm, shows a wavy/cross bedded structure followed by a light green colored, thin (0.5–2 cm) parallel laminated structure (Fig. 4). Thinner (<5 cm) deposits in contrast lack these structural features and show a more homogenous, structureless upper section following a millimeter thick normally graded base. Terrestrial plant remains are common in Lithotype 1 deposits, with larger fragments (>1 mm) being particularly common in thicker (>20 cm) deposits (Fig. 4). Occasionally Lithotype 1 beds are red in color, and apart from the above-mentioned characteristics, are associated with particularly high MS values, Fe count rates, and Fe/Ti ratios. Such beds occur between 19.1–18.9 and 16.5–14.1 m (Fig. 3). Lithotype 1 is much more abundant compared to Lithotype 2 and comprises ~75 % of core Co1230 in form of 99 individual deposits.
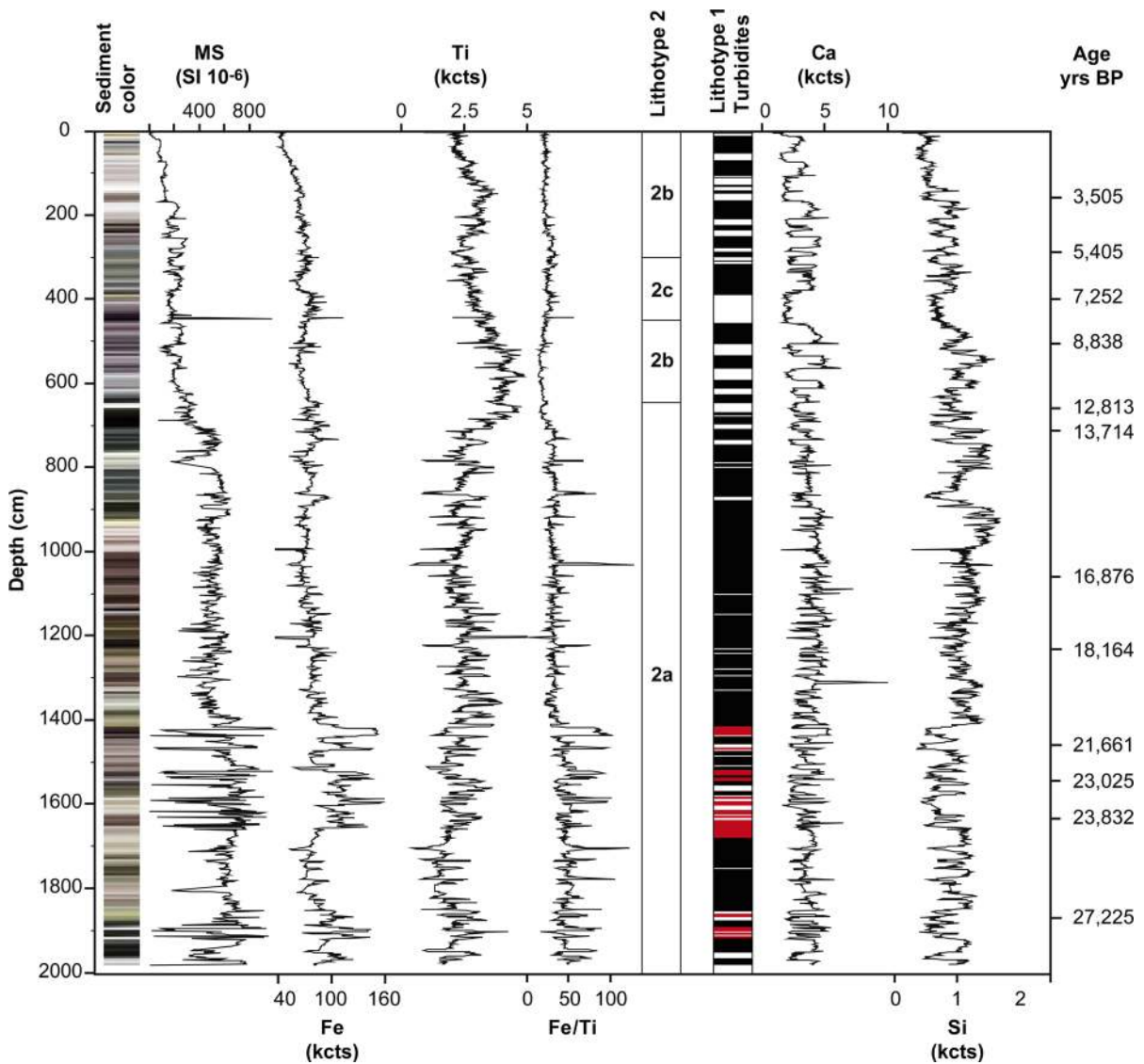
**Fig. 3** Synthetic sediment color (*contrast* and *brightness* increased), magnetic susceptibility (MS), element intensities (Fe, Ti, Ca, Si) displayed in kilo counts (kcts), occurrence of turbidites/Lithotype 1 deposits in core Co1230 (*black*), their *red*/oxidized variety (*red*), and pelagic muds/Lithotype 2 deposits (*white*) occurring interspersed with turbidites, as well as chronostratigraphic information from radiocarbon dating displayed in calibrated years before present (yrs BP). (Color figure online)

Lithotype 2 comprises the remaining ∼25 % of core Co1230 and consists of massive to thinly-bedded clayey silts with variable contents of coarse silt to sand, finely dispersed organic matter, and authigenic siderite. Grain-size distribution in Lithotype 2 sediments is bi-modal with peaks centered between ∼5 to 30 and ∼50 to 150 μm (Fig. 5). In keeping with this bimodality, coarse fraction (>50 μm) concentrations vary strongly between 1.6 and 62 vol% with generally elevated concentrations between 19.8 and 11 m (Fig. 5). Based on differences in color, structure, and the amount and type of occurrence of siderite, Lithotype 2 can be subdivided into three sub-lithotypes. Lithotype 2a occurs between 19.8 and 6.4 m with individual beds between 20 and 1 cm in thickness. Lithotype 2a varies in color from rusty red to dark brown, appears massive and shows variable amounts of finely dispersed siderite. Lithotype 2b occurs between
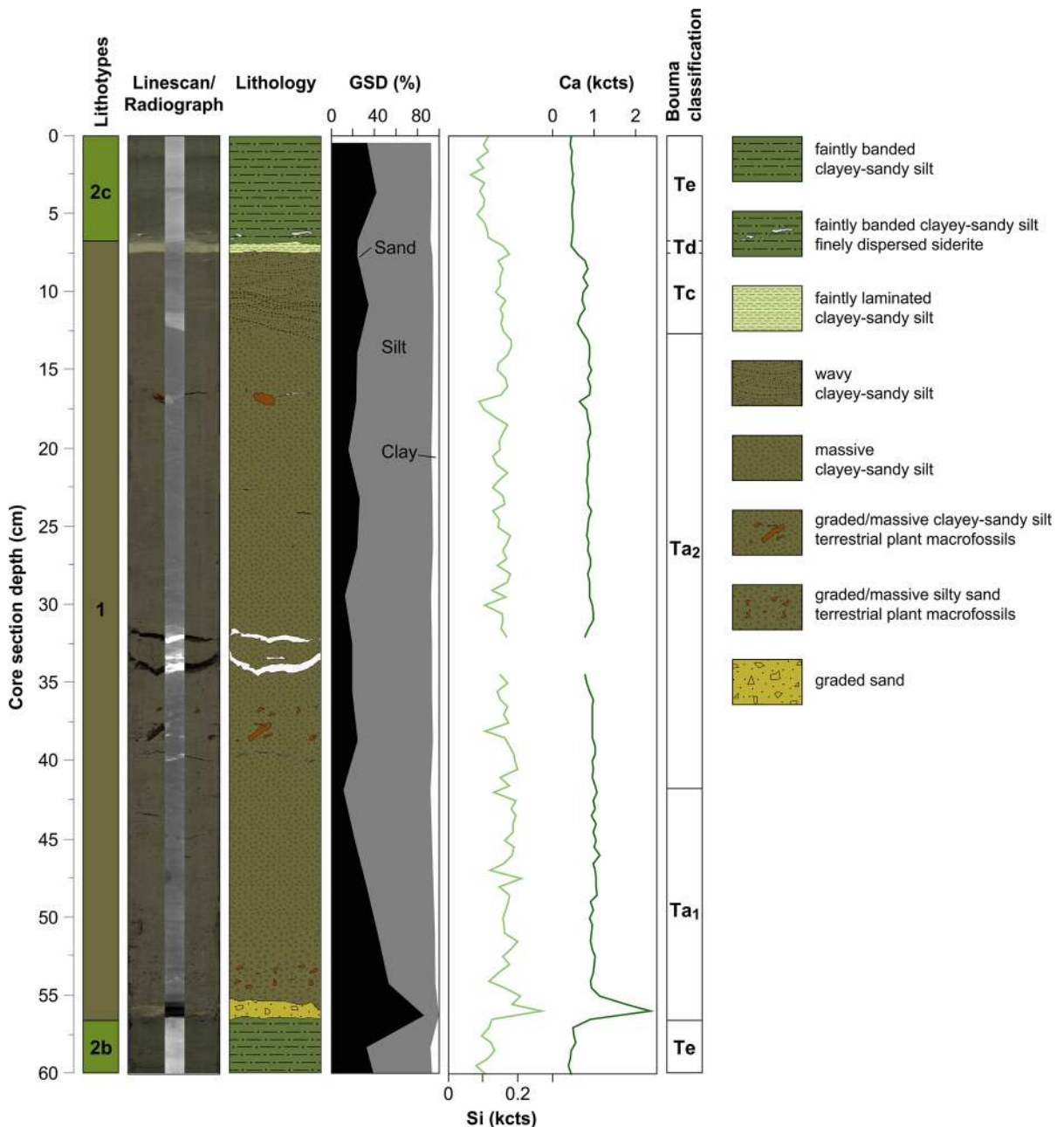
**Fig. 4** Lithological, sedimentological, and geochemical characteristics of a typical turbidite/Lithotype 1 deposit and classification scheme according to Bouma (1962). *GSD* grain-size distribution, *Si* silicon intensities displayed in kilo counts (kcts), *Ca* calcium intensities displayed in kilo counts (kcts), *Te* hemi-pelagic mud, *Ta₁* normal graded sediment, *Ta₂* massive sediment, *Tc* wavy bedded sediment, *Td* parallel laminated sediment. Hence, Si and Ca intensities function as grain-size indicators within Lithotype 1 turbidite deposits. (Color figure online)

6.3–4.5 and 3.0–0 m and is dark green in color, appears thinly bedded (Fig. 4), and shows thicknesses varying between 26 and 2 cm. Lithotype 2c occurs between 4.5 and 3.0 m with thicknesses ranging between 64 and

2 cm. Lithotype 2c is dark to light green in color, faintly banded (Fig. 4), and is further characterized by siderite occurring both as finely dispersed crystals and as individual laminae up to 3 mm thick.
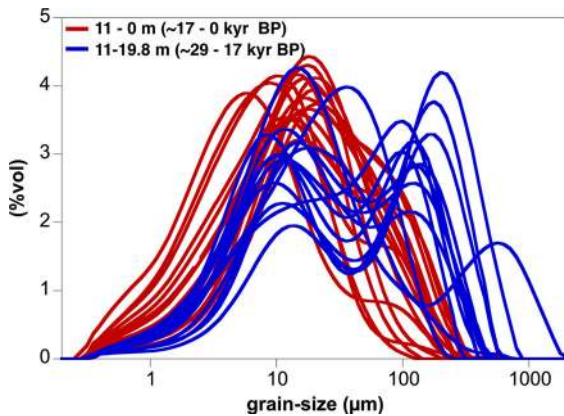
**Fig. 5** Grain-size distribution in pelagic Lithotype 2 sediments showing strong differences in modality. *Blue line color* grain-size distribution in pelagic muds between 19.8 and 11 m subbottom depth (∼29 to 17 kyr BP). *Red line color* grain-size distribution in pelagic muds between 11 and 0 m subbottom depth (∼17 to 0 kyr BP). (Color figure online)

Changes in elemental (Fe, Ti, Si, Ca) intensities and MS values exhibit patterns that are broadly linked to fluctuations in these lithotypes (Fig. 3). MS values and Fe count rates are elevated between 19.8 and 6.5 m relative to 6.5–0 m (Fig. 3). In contrast, Ti intensities show the opposite pattern with Ti intensities being relatively low between 19.8 and 6.5 m compared to 6.5 and 0 m. In addition, Ti shows two prominent and broad maxima centered at 6 and 1.5 m with the former being matched by a Fe minimum (Fig. 3). Apart from these broad patterns in MS, Fe, and Ti, there are numerous smaller, centimeter-scale features associated with the occurrence of Lithotype 1 sediments, marked by higher Ca and Si and lower Ti intensities (Fig. 3). Elevated Ca and Si intensities particularly occur within the coarse-grained basal part of Lithotype 1 sediments (Fig. 4) that primarily consists of serpentine and minor abundances of ultramafic mineral species. Ca and Si intensities therefore function as a sensitive high-resolution indicator for Lithotype 1 deposits and grain-size variability within these deposits. Correlation of MS, Fe, and Fe/Ti patterns with Lithotype 1 deposits is generally less obvious except for the intervals between 19.1–18.9 and 16.5–14.1 m where the red variety of Lithotype 1 deposits occurs (Fig. 3). A decreasing trend in element intensities visible between 4 and 0 m of the core is likely a result of a downcore decrease in water content and associated changes in XRF attenuation (Russell et al. 2014).

Age-model and sedimentation rate

The age-depth model calculated for core Co1230 after excluding Lithotype 1 event deposits indicates a fairly linear age-depth relationship and a basal age of 28.8 calibrated kiloyears before 1950 (hereafter kyr BP; Table 1; Fig. 6a). Comparison of magnetic susceptibility profiles from cores TOW9 and Co1230, plotted against their individual age-models, are in tune and indicate that the reservoir correction established for core TOW9 is also applicable to core Co1230 (Electronic Supplementary Material ESM 1). Sedimentation rates show a pattern with relatively constant and low ($0.11$–$0.17$ mm year$^{-1}$) rates between 28.8 and 14.5 kyr BP and lowest sedimentation rates centered at 18.7 kyr BP. Between ∼17.5 and 10.5 kyr BP sedimentation rates show a gentle increase followed by a more rapid increase starting ∼10.5 and culminating at 8.3 kyr BP, with the highest sedimentation rates ($0.32$ mm year$^{-1}$) of the entire record. Between 8.3 and 6.0 kyr BP sedimentation rates decrease rapidly and remain relatively constant and high ($>0.2$ mm year$^{-1}$) between 6.0 kyr BP and the top of the sequence. Reinserting Lithotype 1 event deposits with constant depositional ages into the age-depth calculation for core Co1230 leads to significantly higher ($1.63$–$0.44$ mm year$^{-1}$) sedimentation rates, with generally high rates ($>0.7$ mm year$^{-1}$) between ∼29 and 14 and lower ($<0.7$ mm year$^{-1}$) between 14 and 0 kyr BP (Fig. 6b). Peak sedimentation rates (∼$1.6$ mm year$^{-1}$) are centered at ∼16 kyr BP.

**Discussion**

Depositional modes in Lake Towuti's northern basin

Based on sedimentological, geochemical, and seismic datasets we can identify two different depositional processes leading to the formation of Lithotype 1 and 2 deposits in Lake Towuti's central northern basin.

Lithotype 1 sediments, with their characteristic features of a sharp basal contact, normal grading fading out into a more homogenous and sometimes wavy bedded and parallel laminated top section, coarse grain-size, and a composition showing high abundances of angular siliciclastic grains and terrestrial plant macrofossils (Fig. 4), indicative for
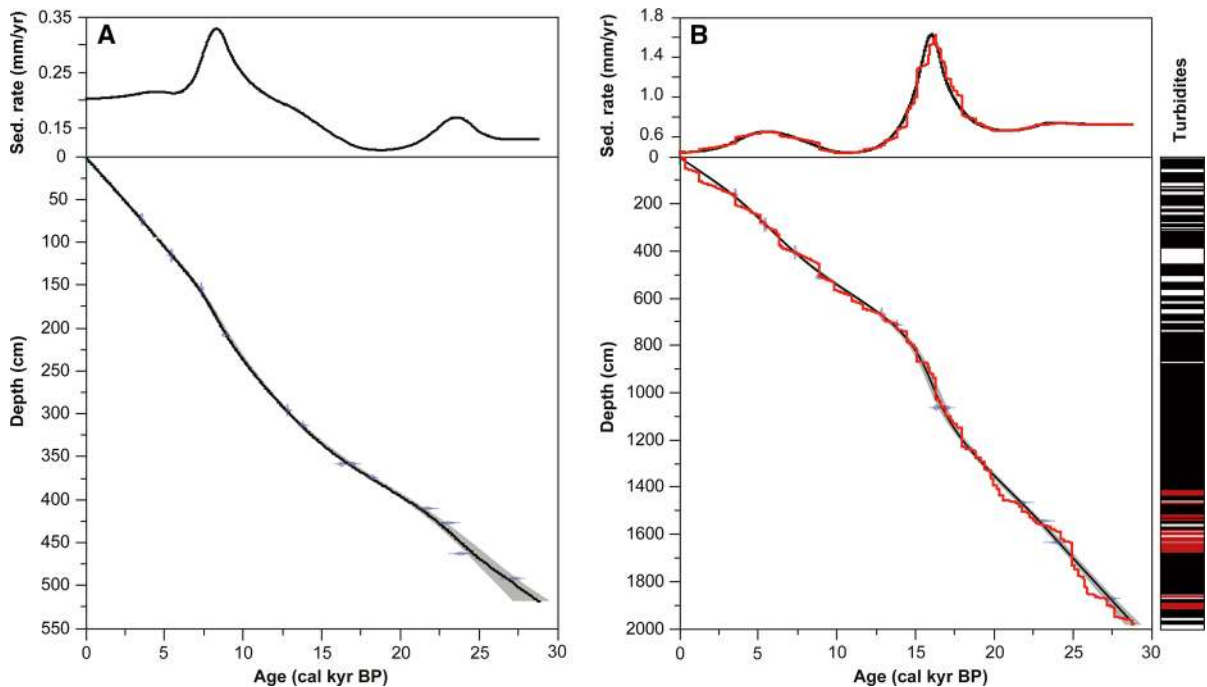
**Fig. 6** Age-depth model and sedimentation rates for core Co1230 without event (Lithotype 1 turbidites) deposits (**a**) and after inserting event deposits with constant ages (**b**)

relatively high transport energies at great water depths, are interpreted as turbidite deposits/Bouma-sequences (Bouma 1962). Depositional processes that involve turbidity currents and/or hyperpycnal flows are supported by seismic data, which reveal a flat basin morphology, thinly spaced high amplitude reflectors, and wedging out of strata towards the basin margins, indicating ponding turbidites (Fig. 2; Adams et al. 2001; Wirth et al. 2011). Due to the coarse-grained character, angular grain shapes, and high amounts of millimeter- to centimeter-sized terrestrial plant macro-fossils we infer that the majority of sediments deposited in these turbidites originates from the Mahalona River and/or its delta slopes (Figs. 1, 2). Seismic data support this source, as sediments draping bedrock highs to the south and east are relatively acoustically transparent with reflections that can be correlated to the fine clays and silts typical of sediments observed elsewhere in the basin.

Discriminating whether turbidites originate from turbidity currents induced by mass movement processes or hyperpycnal flows induced by high volume river discharge events is not straightforward. Turbidites originating from both types of processes

generally produce deposits characterized by normal gradation from sand to silt and clay. Despite these general features characteristic for both processes, discharge induced hyperpycnal flows can also produce deposits with several stacked graded intervals and/or inversely graded intervals related to the temporal waxing and waning of discharge volumes during heavy precipitation/runoff events (Mulder and Alexander 2001; Mulder et al. 2001; Gilli et al. 2013). Mass movement related turbidites, in contrast, often show a thin normal graded base, followed by a thicker homogenous section and/or cross-bedded section (Siegenthaler and Sturm 1991; Beck 2009) as a result of the focused release of the sediment in a very short time (Mulder et al. 2003). In addition and as a common rule, turbidites resulting from mass movement processes typically show greater thicknesses than turbidites resulting from discharge-induced processes (Siegenthaler and Sturm 1991; Sturm et al. 1995; Gorsline et al. 2000). This is a result of the difference in sediment volumes mobilized/transported during discharge induced hyperpycnal flows and mass movement processes, with the latter typically being associated with the mobilization of much larger

sediment volumes. Depositional environments with a strong contribution of discharge related hyperpycnal flow deposits typically show sediment sequences with a characteristic bedding/lamination composed of individual, centimeter to millimeter thick, flood deposits with individual thicknesses of these deposits being controlled by the magnitude and/or duration of the heavy precipitation/flood event (Wirth et al. 2011; Glur et al. 2013); mass movement deposits often achieve much greater thicknesses. Another criterion for the differentiation of turbidites is the composition of the deposit: discharge induced hyperpycnal flow deposits consist predominantly of allochthonous sediments while those originating from mass movement processes reflect the composition of sediment charged, critically inclined basin slopes that function as the source of the sliding mass. The composition of these deposits is therefore strongly source dependent and can vary from pure autochthonous sediments, if the sliding mass originates from slopes charged with hemipelagic sediments, to predominatly allochthonous sediments, if the sliding mass originates from slopes charged with riverine sediments such as delta slopes. Therefore, turbidites originating from delta slope failures can also exhibit a composition dominated by allochthonous/riverine materials (Gilli et al. 2013; Hilbe and Anselmetti 2014).

Based on these criteria, the lithological characteristics of Lithotype 1 deposits (Fig. 4), and evidence for frequent mass wasting from seismic data (Fig. 2B) we interpret turbidites in Lake Towuti's northern basin to be primarily a result of turbidity currents ignited by mass movement processes sourced from the slopes of the Mahalona River Delta. In this case the incorporation of oxidized (shallow water and/or aerially exposed) sediments would explain the red colored, iron oxide rich variety of turbidites observed in the deeper sections of core Co1230 (Fig. 3). Direct correlation of turbidites deposited in the deep basin to their proximal mass movement deposits emplaced on the toe of the Mahalona Delta slopes is hampered by poor acoustic penetration over the delta slopes (Fig. 2). Despite the lack of direct correlation we suggest that turbidite thickness in Lake Towuti's northern basin is, in addition to source proximity and the direction of the turbidity current, a function of the volume mobilized during the respective mass movement event.

Relatively homogenous Lithotype 2 sediments, composed of clastic debris, finely dispersed organic matter, and authigenic mineral phases can best be described as a product of hemi-pelagic sedimentation in Lake Towuti's deep northern basin. Grain-size distributions in Lithotype 2 vary through the core, with the bi-modal grain-size composition (Fig. 5), characterized by peaks in the fine silt and sand-sized range (>50 μm), implying that lateral transport processes, in addition to suspension fallout through the water column, at times contribute to pelagic sedimentation at coring site Co1230. In the case of Lithotype 2 sediments, lateral transport processes could involve either distal products of mass movement or flood induced turbidity currents. In addition, variable abundances of coarse-grained particles at central basin sites are commonly explained by lake-level fluctuations and associated changes of shore-line proximity to the coring site (Bird et al. 2014). Lake-level induced changes in shore-line proximity would increase the probability of material from hyperpycnal flows and interflows to reach site Co1230. Higher abundances of the coarse fraction in the pelagic sediments of Lithotype 2 may therefore indicate a stronger relative contribution of more distal and/or low volume mass movement induced turbidity currents and/or hyperpycnal flows to pelagic sedimentation at site Co1230.

Temporal variations of Ti (terrestrial runoff) and Fe (redox processes) intensities and MS values (preservation of magnetite) in core Co1230 (Fig. 3) are well correlated to variations of these parameters measured in piston core TOW9 (Fig. 1B; Russell et al. 2014; Costa et al. 2015; Tamuntuan et al. 2015). While piston coring site TOW9 is also located in Towuti's northern basin it is widely protected from sediment delivery originating from the Mahalona River and its delta (Fig. 1B). This implies that climatic controls on sediment delivery, geochemistry, and post-depositional sediment alteration are not significantly affected by the contribution of laterally transported/remobilized sediments at site Co1230.

Mechanisms explaining variability of lateral transport processes and turbidite recurrence rates during the past 29 kyrs

The amount of the coarse fraction in pelagic sediments as well as cumulative turbidite thicknesses and recurrence rates in Lake Towuti's northern basin vary strongly during the past ∼29 kyrs. Broadly, high coarse fraction amounts, turbidite recurrence rates,

and cumulative turbidite thicknesses occur between ∼29 and 16 kyr BP, and lower values occur between ∼11 and 0 kyr BP (Fig. 7). Coarse fraction amounts decrease gradually from 17 to 11 kyr BP and remain relatively low and constant for the remainder of the record (Fig. 7). The turbidite record is characterized by peak frequencies (>6 turbidites 1000 years⁻¹) and cumulative thicknesses (>1.1 m 1000 years⁻¹) between ∼26 to 24 and ∼18 to 16 kyr BP (Fig. 7). In contrast, the period between ∼11 and 0 kyr BP is, with exception of the period between ∼7 and 5 kyr BP, characterized by relatively low turbidite frequencies (<2 turbidites/1000 years) and low cumulative turbidite thicknesses (<0.6 m 1000 years⁻¹, Fig. 7). In light of independent geochemical evidence from the carbon isotope composition of terrestrial leaf waxes and elemental runoff indicators for aridity from ∼30 to 16 kyr BP in Lake Towuti (Fig. 7; Russell et al. 2014), we find that the relative contribution of sediments transported laterally in Towuti's deep northern basin is positively correlated to dry periods.

The strong correlation with dry periods hints at changes in lake-level and shore-line proximity as the primary mechanism controlling increased deposition of laterally transported sediments in Lake Towuti's northern basin. In line with similar considerations made for the behavior of marine delta and slope systems (Einsele 1996; Muto and Steel 2002; Lee 2009) we suggest that shore-line regression during falling and lake-level lowstand stages leads to partial, or even complete, exposure of the Mahalona River Delta topset, allowing for a variety of mass-movement processes that cause enhanced sediment transport and deposition of Lithotype 1 turbidites at our core site. Slope stability is likely to decrease in this lake-level forced prograding delta system due to increased rates of sediment accumulation and underconsolidation as well as oversteepening, resulting in excess pore pressure and increased sheer stresses on the frontal delta slopes triggering mass movements (Lee 2009). Deeper incision of active river channels into and wave-induced erosion of high-stand sediment deposits will also result in increased sediment transport and deposition. These mechanisms require a sustained, but not necessarily similarly strong, discharge from the Mahalona River during dry compared to wet phases in order to transport sediment to the frontal delta slopes. A sustained discharge from the Mahalona River is confirmed by elemental tracers (Costa et al. 2015) and

a somewhat wetter climate in the upstream catchment of the Mahalona River during the dry last glacial (Wicaksono et al. 2015).

In addition, lake-level drops may cause temporary disequilibria between confining pressure and pore pressure in less permeable sediments and may lead to increased ebullition and discharge of biogenic gases from organic rich delta sediments, which would increase the susceptibility of delta slopes to gravitational failure (Moernaut et al. 2010). Spontaneous delta collapses resulting from a buildup of excess pore pressure due to rapid sediment loading and lake-level drops in combination with oversteepening as a result of increased sediment charging on the frontal delta slopes (Sultan et al. 2004; Girardclos et al. 2007) are likely one of the main causes for gravitational mass flows and turbidite deposition. When considering the specific setting of Lake Towuti, additional factors increasing stresses and/or lower sediment strength, such as earthquakes, high-volume river discharge events, storm waves, biogenic pore gas charging, seasonal lake-level fluctuations, as well as complex interactions of these factors may also contribute to Mahalona Delta slope failure (Coleman and Prior 1988; Hampton et al. 1996).

Sustained Mahalona River discharge along with erosional processes during lowstand stages would also promote a basinward progradation of the Mahalona Delta. Suspended matter from heavy discharge events as well as flood induced turbidity currents would in this case be more likely to reach more distal parts of the basin, explaining the deposition of coarse sediments and grain-size bimodality in Lithotype 2 beds. Rising and lake-level highstand stages establish accommodation space on the delta topset, resulting in a reduction of sediment transport to and deposition on frontal delta slopes and the distal basin and a shift to more pelagic sedimentation in the upper 11 m of Lithotype 2.

Lake-level variability at Lake Towuti and implications for the regional hydroclimate during the past 29 kyrs

We interpret increased amounts of laterally transported sediments at coring site Co1230 as being primarily a result of lake-level low-stands in Lake Towuti. Therefore, we suggest that the coarse fraction amount as well as turbidite recurrence rates and
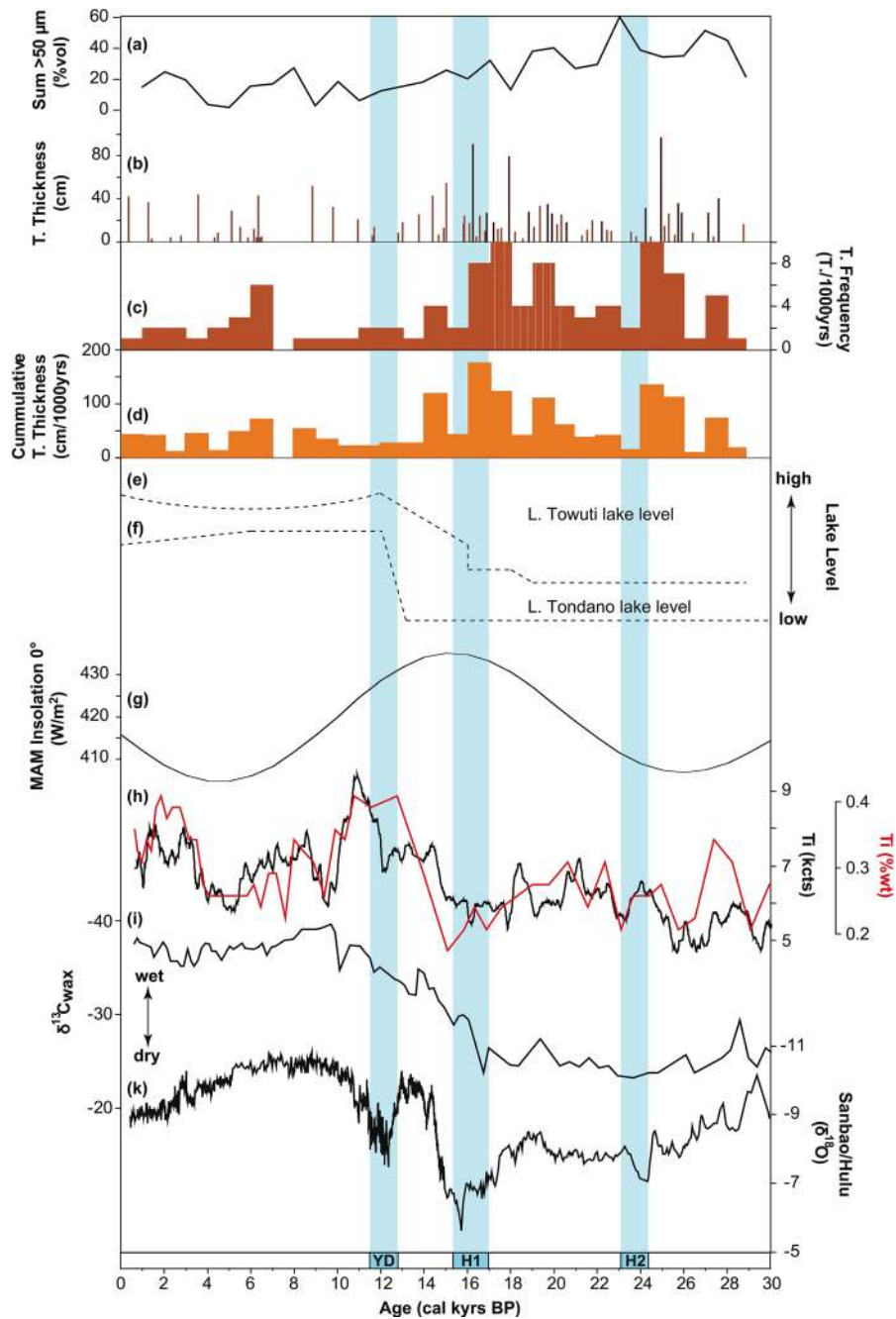
Fig. 7 Comparison of sedimentological indicators for lake-level variability at Lake Towuti to hydroclimate proxy time series from Lake Towuti and paleoclimate records from nearby regions: *a* coarse fraction (>50 µm) concentrations in pelagic/Lithotype 2 sediments of core Co1230, *b* turbidite occurrence and thicknesses in core Co1230 (*brown* individual turbidites, *black* consecutive turbidites), *c* turbidite (T.) frequencies/recurrence rates per 1000 years in core Co1230, *d* cumulative turbidite (T.) thicknesses per 1000 years in core Co1230, *e* tentative lake-level reconstruction for Lake Towuti, with *arrows* marking phases of suggested rapid drops in lake-level, *f* lake-level reconstruction from Lake Tondano, N-Sulawesi, Indonesia (Dam et al. 2001), *g* wet season (Lake Towuti)/March–April–May (MAM) mean insolation at 0° (Laskar et al. 2004), *h* titanium (Ti) intensities (*kcts* kilo counts) and percent by weight (wt%) from core TOW9 (Russell et al. 2014), *i* carbon isotope composition of terrestrial leaf waxes (δ13Cwax) from core TOW9 (Russell et al. 2014), and *k* Hulu cave δ18O records from China (Wang et al. 2001). *YD* Younger Dryas, *H1* Heinrich Event 1, *H2* Heinrich Event 2. (Color figure online)

cumulative thicknesses are indicators for the magnitude of relative lake-level changes. Highest turbidite recurrence rates and cumulative thicknesses may also indicate rapidly falling and/or lowest lake-levels in Lake Towuti (Fig. 7).

Based on the sedimentary indicators we infer relatively low lake-levels at Lake Towuti during the last glacial between ~29 and 16 kyr BP, gradually increasing lake-levels during the transition from the last glacial into the Holocene between ~16 and 11 kyr BP, and highest lake-levels during the Holocene between ~11 and 0 kyr BP (Fig. 7). Lowest lake-levels are inferred for the period ~29 and 19 kyr BP, and more rapid lake-level drops are inferred for the periods ~26 to 24 and ~18 to 16 kyr BP based on the abundance of exceptionally thick and frequent turbidite successions (Fig. 7). The gradual decrease in coarse fraction amounts and turbidite deposition after ~16 kyr BP indicates a rise in lake-level following the lowstand during the last glacial period. Following this lake-level rise at the end of the last glacial period, the Holocene experienced only subtle lake-level fluctuations, although a somewhat muted Holocene lowstand is indicated for the period ~8 to 5 kyr BP (Fig. 7).

The sedimentologically inferred lake-level record of Lake Towuti is correlated with terrestrial leaf wax carbon isotope ($\delta^{13}C_{wax}$), titanium (Ti), and redox sensitive metal records from core TOW9 (Figs. 1, 7) representing vegetation structure, terrestrial runoff intensity, and water column mixing, respectively (Russell et al. 2014; Costa et al. 2015). Inferred lower lake-levels during the last glacial coincide with an open forest ecosystem with dry adapted $C_4$ grasses, reduced terrestrial runoff (Russell et al. 2014), a well-mixed water column (Costa et al. 2015), and lake-level lowstands at Lake Tondano in northern Sulawesi (Dam et al. 2001; Fig. 7). Reduced terrestrial runoff and a vegetation dominated by $C_4$ grasses during the last glacial are interpreted to reflect a significant reduction in annual rainfall as a result of both reduced wet season precipitation and runoff (low Ti) and a longer and more pronounced dry season causing water stress (enriched $\delta^{13}C_{wax}$). High-latitude northern hemisphere ice-sheet forcing on the position of the ITCZ and Austral-Asian monsoon systems has been suggested to be the primary mechanism controlling the reduction in annual precipitation during the last glacial (Russell et al. 2014). Deeper mixing of Lake Towuti's

water column during the last glacial is thought to be caused by enhanced evaporative cooling of surface waters due to a longer and more pronounced dry season (Costa et al. 2015, Dubois et al. 2014). A longer and more pronounced dry season, along with reduced wet season precipitation, in combination with an open forest/grassland vegetation cover would consequently lead to increased evaporation from lake Towuti's catchment soils thus further reducing terrestrial runoff to the lake. We therefore explain the last glacial lake-level lowstand at Lake Towuti to be the result of the combined effects of reduced annual precipitation and enhanced evaporation from the lake surface and catchment soils, with the timing of major transitions controlled by glacial-interglacial climate boundary conditions.

Periods with inferred rapid lake-level drops between ~26 to 24 and ~18 to 16 ky BP are, however, not pronounced in the $\delta^{13}C_{wax}$, Ti, and redox sensitive metal datasets (Fig. 7). This discrepancy may be related to differences in the sensitivity of the geochemical datasets during these periods. Nevertheless, the occurrence of frequent, thick turbidite successions points to rapid and possibly short-lived lake-level drops. Interestingly, the timing of these rapid lake-level drops is, within the error of our age-model (Table 1, Fig. 6), coincident with significant dry spells in the Austral-Asian Monsoon domain as recorded in speleothem records from China (32°30′N, 119°10′E; Wang et al. 2001; Fig. 7) and Borneo (4°N, 115°E; Partin et al. 2007; Carolin et al. 2013) and marine records offshore Sumatra (3°N–0°50′S, 96–99°50′E; Mohtadi et al. 2014) and Java (8°41′S, 112°52′E; Mohtadi et al. 2011). These dry spells have been suggested to correspond to North Atlantic Heinrich events 2 and 1 (Wang et al. 2001). A somewhat subdued millennial scale dry spell, coinciding with the Younger Dryas (YD), is recorded in the Chinese speleothem records and marine records from offshore Sumatra and Java (Wang et al. 2001; Mohtadi et al. 2011, 2014) but is missing in the Borneo speleothems (Partin et al. 2007; Carolin et al. 2013) and at Lake Towuti (Russell et al. 2014, this study).

Climate anomalies associated with Heinrich events and the YD originate in the North Atlantic region as a result of the slowdown of the Atlantic Meridional Overturning Circulation (AMOC) and reduction of North Atlantic Deep Water (NADW) formation due to iceberg surges and/or freshwater forcing (Rahmstorf

2002; Condron and Winsor 2012) and induce, through increases in sea ice coverage and albedo, widespread northern hemisphere cooling (Chiang and Bitz 2005). Widespread northern hemisphere cooling is thought to drive a southward migration of the ITCZ, which leads to drying in most of the northern and wetter conditions in the southern tropics (Chiang and Bitz 2005; Broccoli et al. 2006). The drying recorded at Lake Towuti and marine records from offshore Sumatra and Java, which is supported by modeling studies (Pausata et al. 2011; Mohtadi et al. 2014), imply that drying during Heinrich events 2 and 1 also affected the southern tropics of the maritime continent. Interestingly, despite the similarity of the underlying mechanisms of Heinrich events 2 and 1, only the latter is commonly referred to as having caused significant climate anomalies in the tropics (Stager et al. 2011). Our dataset implies, however, that both Heinrich events 2 and 1 may have led to reductions in rainfall in the tropics of the maritime continent.

The variable response of the records from the Austral-Asian monsoon regions to the Heinrich and YD climate anomalies is likely related to the style and characteristics of each individual event in the North Atlantic and the atmospheric processes involved in translating the climate signal into the Austral-Asian monsoon domains (Mohtadi et al. 2014). Iceberg discharge into the North Atlantic during Heinrich events 2 and 1 led to an almost complete shutdown of North Atlantic Deep Water (NADW) formation, in contrast to freshwater forcing during the YD (Böhm et al. 2015). Stronger cooling in the North Atlantic region during Heinrich events 2 and 1 compared to the YD, along with an ice sheet geometry and extent close to last glacial maximum conditions, may therefore explain the differences in magnitude and spatial extent of these climate anomalies in the Austral–Asian monsoon domain.

The inferred lake-level highstand period 11–0 kyr BP is in agreement with a generally wetter Holocene climate as indicated by a closed canopy rainforest ecosystem, strong terrestrial runoff (Fig. 7; Russell et al. 2014), and a poorly ventilated water column at Lake Towuti (Costa et al. 2015). Moreover, subtle Holocene lake-level variability, with a somewhat higher lake-level during the Early- and Late-Holocene and a lowstand between $\sim 8$ and 5 kyr BP is corroborated by slight enrichment in $\delta^{13}C_{wax}$, reduced Ti concentrations, and changes in redox sensitive metal

records, which indicate a muted increase in dry season water stress during the Mid- compared to the Early- and Late-Holocene, reduced wet season runoff, and increased evaporative cooling (Fig. 7). The temporal evolution of precipitation recorded at Lake Towuti during the Holocene therefore appears to be primarily controlled by the strength of equatorial wet season (March–April–May; MAM) insolation (Fig. 7). The pattern observed at Lake Towuti is also in agreement with precipitation changes recorded in terrestrial runoff and sea surface salinity records from offshore Java (Mohtadi et al. 2011), Sumba (Steinke et al. 2014), the Timor Sea (Kuhnt et al. 2015), and lake-level records from central Australia (Magee et al. 2004), that record rainfall amount associated with the annual passage of the ITCZ and the AISM circulation.

In contrast, speleothem records from the EAM domain (China and Borneo) show a different or even antiphased pattern with that of Towuti (Wang et al. 2001; Partin et al. 2007; Carolin et al. 2013). At Borneo in particular, oxygen isotope data indicate peak precipitation during the Mid-Holocene and reduced precipitation during the Early- and Late-Holocene (Partin et al. 2007; Carolin et al. 2013). Peak precipitation during the Early Holocene observed in Chinese cave records (Wang et al. 2001) is thought to be a result of enhanced warming of the northern hemisphere in response to increased summer insolation, (Shakun et al. 2012) and an associated northward shift of the ITCZ (Kuhnt et al. 2015). In this context the reduction in AISM precipitation during the Mid Holocene observed at Towuti could be a result of a northward shift of the ITCZ due to relatively low (high) southern (northern) hemisphere insolation and higher temperatures in the northern relative to the southern hemisphere (Wanner et al. 2008; Shakun et al. 2012). However, the peak in mid-Holocene precipitation at Borneo is interpreted to reflect intensification of the equatorial hydrological cycle related to southward ITCZ migration and peak insolation in boreal fall. Due to its equatorial location, Lake Towuti experienced the same insolation forcing, yet our records indicate an opposite hydrological response, indicating significant heterogeneity in mid-Holocene climates in this region. The intensification of the AISM from the dry Mid- to the wet Late Holocene is likely related to an orbitally induced increase in southern hemisphere summer insolation and associated transition of the ITCZ from the northern into the

southern tropics (Mohtadi et al. 2011; Kuhnt et al. 2015). We therefore suggest that, while major climate boundaries at Lake Towuti are shaped by varying glacial-interglacial climate boundary conditions, hemispheric temperature contrasts and astronomic forcing exert the primary control on regional hydrology and AISM intensity during the Holocene/interglacials in the maritime continent and at Lake Towuti.

## Conclusions

Detailed lithological and sedimentological analyses along with seismic reflection data provide insight into depositional processes in Lake Towuti during the past $\sim$29 kyr BP. We find that sedimentation in Towuti's northern basin is affected by strong contributions from lateral gravitational- and discharge-induced sediment transport processes. A succession of 99 turbidites deposited during the past $\sim$29 kyr BP is emblematic for the strong contribution of lateral transport to deposition in Towuti's northern basin. Structural and compositional features of individual turbidite deposits in combination with mass wasting deposits visible in seismic data between the coring site and the Mahalona River Delta imply that turbidites are likely a product of turbidity currents ignited by gravitational mass wasting events originating from the delta. Relatively homogenous muds form the (hemi)pelagic background sediments, reflecting vertical settling of fine-grained sediment through the water column. However, grain-size distribution in these muds is at times bimodal with peaks centered in the fine-silt and middle-sand regions thus further emphasizing the importance of lateral transport to sedimentation.

We utilized geochemical data, coarse fraction amounts in pelagic muds, as well as turbidite recurrence rates and cumulative thicknesses as indicators for the relative contribution of laterally transported sediments to our coring site. Temporal variation in our dataset is correlated to hydroclimatic proxy time series from Lake Towuti and other regional records. Dry phases in these regional proxy time-series are correlated to phases of stronger contribution from lateral transport processes to sedimentation at our coring site. We therefore suggest that lake-level fluctuations and associated changes in sediment delivery exert primary control on the amount of laterally transported sediment reaching our coring site in Lake Towuti's northern basin. Based on our sedimentological dataset we infer that lake-levels were generally low between $\sim$29 and 16, rose gradually between $\sim$16 and 11, and are comparable to modern levels since $\sim$11 kyr BP. Periods of rapid lake-level drops, as indicated by highest turbidite recurrence rates and cumulative thicknesses, are suggested to have occurred between $\sim$26 to 24 and $\sim$18 to 16 kyr BP, coincident with Heinrich events 2 and 1. Detailed seismic and bathymetric surveys in combination with targeted sediment coring in shallow water may enable quantification of lake-level fluctuations and help to calibrate our relative lake-level reconstruction in the future.

## References

Adams E, Schlager W, Anselmetti FS (2001) Morphology and curvature of delta slopes in Swiss lakes: lessons for the interpretation of clinoforms in seismic data. Sedimentology 48:661–679

Alin SR, Cohen AS (2003) Lake-level history of Lake Tanganyika, East Africa, for the past 2500 years based on ostracode-inferred water-depth reconstruction. Palaeogeogr Palaeoclimatol Palaeoecol 199:31–49

Anselmetti FS, Ariztegui D, DeBatist M, Gebhardt AC, Haberzettl T, Niessen F, Ohlendorf C, Zolitschka B (2009) Environmental history of southern Patagonia unraveled by the seismic stratigraphy of Laguna Potrok Aike. Sedimentology 56:873–892

Beck C (2009) Late Quaternary lacustrine paleo-seismic archives in north-western Alps: examples of earthquake-origin assessment of sedimentary disturbances. Earth Sci Rev 96:327–344

Bird BW, Polisar PJ, Lei Y, Thompson LG, Yao T, Finney BP, Bain DJ, Pompeani DP, Steinman BA (2014) A Tibetan lake sediment record of Holocene Indian summer monsoon variability. Earth Planet Sci Lett 399:92–102

Blaauw M (2010) Methods and code for 'classical' age-modelling of radiocarbon sequences. Quat Geochronol 5:512–518

Böhm E, Lippold J, Gutjahr M, Frank M, Blaser P, Antz B, Fohlmeister J, Frank N, Andersen MB, Deininger M (2015) Strong and deep Atlantic meridional overturning circulation during the last glacial cycle. Nature 517:73–76

Bouma AH (1962) Sedimentology of some flysch deposits: a graphic approach to facies interpretation. Elsevier, Amsterdam, p 168

Broccoli AJ, Dahl KA, Stouffer RJ (2006) Response of the ITCZ to Northern Hemisphere cooling. Geophys Res Lett 33:L01702

Cane M, Clement AC (1999) A role for the tropical Pacific coupled ocean-atmosphere system on Milankovitch and millenial timescales. Part II: global impacts. In: Peter U, Clark PU, Robert S, Webb RS, Lloyd D, Keigwin LD (eds) Mechanisms of global climate change at millennial time scales. Geophysical monograph series, vol 112. American Geophysical Union, Washington, pp 373–383

Carolin SA, Cobb KM, Adkins JF, Clark B, Conroy JL, Lejau S, Malang J, Tuen A (2013) Varied response of Western Pacific hydrology to climate forcings over the last glacial period. Science 340:1564–1566

Chiang JCH (2009) The tropics in paleoclimate. Ann Rev Earth Planet Sci 37:263–297

Chiang JCH, Bitz CM (2005) Influence of high latitude ice cover on the marine Intertropical Convergence Zone. Clim Dyn 25:477–496

Clement AC, Cane MA, Seager R (2001) An orbitally driven tropical source for abrupt climate change. J Clim 14:2369–2375

Coleman JM, Prior DB (1988) Mass wasting on continental margins. Ann Rev Earth Planet Sci 16(1):101–119

Condron A, Winsor P (2012) Meltwater routing and the Younger Dryas. Proc Natl Acad Sci 109:19928–19933

Costa KM, Russell JM, Vogel H, Bijaksana S (2015) Hydrological connectivity and mixing of Lake Towuti, Indonesia in response to paleoclimatic changes over the last 60,000 years. Palaeogeogr Palaeoclimatol Palaeoecol 417:467–475

Dam RAC, Fluin J, Suparan P, van Der Kaars S (2001) Palaeoenvironmental developments in the Lake Tondano area (N. Sulawesi, Indonesia) since 33,000 yr BP. Palaeogeogr Palaeoclimatol Palaeoecol 171:147–183

Dubois N, Oppo DW, Galy VV, Mohtadi M, van der Kaars S, Tierney JE, Rosenthal Y, Eglinton TI, Lückge A, Linsley BK (2014) Indonesian vegetation response to changes in rainfall seasonality over the past 25,000 years. Nat Geosci 7:513–517

Einsele G (1996) Event deposits: the role of sediment supply and relative sea-level changes—overview. Sediment Geol 104:11–37

Gasse F, Lédée V, Massault M, Fontes J-C (1989) Water-level fluctuations of Lake Tanganyika in phase with oceanic changes during the last glaciation and deglaciation. Nature 342:57–59

Gilli A, Anselmetti FS, Glur L, Wirth SB (2013) Lake sediments as archives of recurrence rates and intensities of past flood events. In: Schneuwly-Bollschweiler M, Stoffel M, Rudolf-Miklau M (eds) Dating torrential processes on fans and cones—methods and their application for hazard and risk assessment, advances in global change research. Springer, Dordrecht, pp 225–241

Girardclos S, Schmidt OT, Sturm M, Ariztegui D, Pugin A, Anselmetti FS (2007) The 1996 AD delta collapse and large turbidite in Lake Brienz. Mar Geol 241:137–154

Glur L, Wirth SB, Büntgen U, Gilli A, Haug GH, Schär C, Beer J, Anselmetti FS (2013) Frequent floods in the European Alps coincide with cooler periods of the past 2500 years. Nat Sci Rep 3:2770

Golightly JP, Arancibia ON (1979) The chemical composition and infrared spectrum of nickel- and iron-substituted serpentine from a nickeliferous laterite profile, Soroako, Indonesia. Can Mineral 17:719–728

Gorsline DS, De Diego T, Nava-Sanchez EH (2000) Seismically triggered turbidites in small margin basins: Alfonso Basin, Western Gulf of California and Santa Monica Basin, California Borderland. Sed Geol 135:21–35

Haberzettl T, Fey M, Lücke A, Maidana N, Mayr C, Ohlendorf C, Schäbitz F, Schleser GH, Wille M, Zolitschka B (2005) Climatically induced lake level changes during the last two millennia as reflected in sediments of Laguna Potrok Aike, southern Patagonia (Santa Cruz, Argentina). J Paleolimnol 33:283–302

Haffner GD, Hehanussa PE, Hartoto D (2001) The biology and physical processes of large lakes of Indonesia: Lakes Matano and Towuti. In: Munawar M, Hecky RE (eds) The Great Lakes of the World (GLOW): food-web, health, and integrity. Backhuys Publishers, Leiden, pp 129–155

Hall R (1996) Reconstructing Cenozoic SE Asia. In: Hall R, Blundell DJ (eds) Tectonic evolution of SE Asia, vol 106. Geological Society of London Special Publication, London, pp 153–184

Hamilton W (1979) Tectonics of the Indonesian region. U.S.G.S. professional paper, 1078

Hampton MA, Lee HJ, Locat J (1996) Submarine landslides. Rev Geophys 34(1):33–59

Hilbe M, Anselmetti FS (2014) Signatures of slope failures and river-delta collapses in a perialpine lake (Lake Lucerne, Switzerland). Sedimentology 61:1883–1907

Kadarusman A, Miyashita S, Maruyama S, Parkinson CD, Ishikawa A (2004) Petrology, geochemistry and paleogeographic reconstruction of the East Sulawesi Ophiolite, Indonesia. Tectonophysics 392:55–83

Kuhnt W, Holbourn A, Xu J, Opdyke B, De Decker P, Röhl U, Mudelsee M (2015) Southern Hemisphere control on Australian monsoon variability during the late deglaciation and Holocene. Nat Comm 6:5916

Laskar J, Robutel P, Joutel F, Gastineau M, Correia ACM, Levrard B (2004) A long-term numerical solution for the insolation quantities of the Earth. Astron Astrophys 428:261–285

Lee HJ (2009) Timing of occurrence of large submarine landslides on the Atlantic Ocean margin. Mar Geol 264:53–64

Lehmusluoto P, Machbub B, Terangna N, Rusmiputro S, Achmad F, Boer L, Brahmana SS, Priadi B, Setiadji B, Sayuman O, Margana A (1995) National inventory of the major lakes and reservoirs in Indonesia. General limnology, FAO-FINNIDA

Lindhorst K, Vogel H, Krastel S, Wagner B, Hilgers A, Zander A, Schwenk T, Wessels M, Daut G (2010) Stratigraphic analysis of lake level fluctuations in Lake Ohrid: an

integration of high resolution hydro-acoustic data and sediment cores. Biogeosciences 7:3531–3548

Magee JW, Miller GH, Spooner NA, Questiaux D (2004) Continuous 150 k.y. monsoon record from Lake Eyre, Australia: insolation-forcing implications and unexpected Holocene failure. Geology 10:885–888

Moernaut J, Verschuren D, Charlet F, Fagot M, De Batist M (2010) The seismic stratigraphic record of lake-level fluctuations in Lake Challa: hydrological stability and change in equatorial East Africa over the last 140 kyr. Earth Planet Sci Lett 290:214–223

Mohtadi M, Oppo DW, Steinke S, Stuut J-BW, De Pol-Holz R, Hebbeln D, Lückge A (2011) Glacial to Holocene swings of the Australian–Indonesian monsoon. Nat Geosci 4:540–544

Mohtadi M, Prange M, Oppo DW, De Pol-Holz R, Merkel U, Zhang X, Steinke S, Lückge A (2014) North Atlantic forcing of tropical Indian Ocean climate. Nature 509:76–80

Mulder T, Alexander J (2001) The physical character of subaqueous sedimentary density flows and their deposits. Sedimentology 48:269–299

Mulder T, Migeon S, Savoye B, Faugères J-C (2001) Inversely graded turbidite sequences in the deep Mediterranean: a record of deposits from flood-generated turbidity currents? Geo Mar Lett 21:86–93

Mulder T, Syvitski JPM, Migeon S, Faugères J-C, Savoye B (2003) Marine hyperpycnal flows: initiation, behavior and related deposits. A review. Mar Pet Geol 20:861–882

Muto T, Steel RJ (2002) In defense of shelf-edge delta development during falling and lowstand of relative sea level. J Geol 110:421–436

Partin JW, Cobb KM, Adkins JF, Clark B, Fernandez DP (2007) Millennial-scale trends in west Pacific warm pool hydrology since the Last Glacial Maximum. Nature 449:452–455

Pausata FSR, Battisti DS, Nisancioglu KH, Bitz CM (2011) Chinese stalagmite $\partial^{18}$O controlled by changes in the Indian monsoon during a simulated Heinrich event. Nat Geosci 4:474–480

Pierrehumbert RT (1999) Subtropical water vapor as a mediator of rapid global climate changes. In: Clark PU, Webb RS, Keigwin LD (eds) Mechanisms of global climate change at millennial time scales. Geophysical monograph series, vol 112. American Geophysical Union, Washington, pp 339–361

Rahmstorf S (2002) Ocean circulation and climate during the past 120,000 years. Nature 419:207–214

Reimer PJ, Bard E, Bayliss A, Beck JW, Blackwell PG, Bronk Ramsey C, Buck CE, Edwards RL, Friedrich M, Grootes PM, Guilderson TP, Haflidason H, Hajdas I, Hatté C, Heaton TJ, Hoffmann DL, Hogg AG, Hughen KA, Kaiser KF, Kromer B, Manning SW, Niu M, Reimer RW, Richards DA, Scott EM, Southon JR, Turney CSM, van der Plicht J (2013) IntCal13 and Marine13 radiocarbon age calibration curves, 0–50,000 years cal BP. Radiocarbon 55:1869–1887

Rethemeyer J, Dewald A, Fülöp R, Hajdas I, Höfle S, Patt U, Stapper B, Wacker L (2013) Status report on sample preparation facilities for $^{14}$C analysis at the new Colog-neAMS centre. Nucl Instrum Meth B 294:168–172

Rintelen T, Rintelen K, Glaubrecht M, Schubart CD, Herder F (2012) Aquatic biodiversity hotspots in Wallacea: the species flocks in the ancient lakes of Sulawesi, Indonesia.

In: Goer DJ, Johnson KG, Richardson JE, Rosen BR, Williams LR, Williams ST (eds) Biotic evolution and environmental change in Southeast Asia. Cambridge University Press, Cambridge, pp 290–315

Russell JM, Bijaksana S (2012) The Towuti Drilling Project: paleoenvironments, biological evolution, and geomicrobiology of a Tropical Pacific lake. Sci Drill 14:68–71

Russell JM, Vogel H, Konecky BL, Bijaksana S, Huang Y, Melles M, Wattrus N, Costa K, King JW (2014) Glacial forcing of central Indonesian hydroclimate since 60,000 y B.P. Proc Natl Acad Sci 111:5100–5105

Scholz CA, Johnson TC, Cohen AS, King JW, Peck JA, Overpeck JT, Talbot MR, Brown ET, Kalindekafe L, Amoako PYO, Lyons RP, Shanahan TM, Castñeda IS, Hell CW, Forman SL, McHargue LR, Beuning KR, Gomez J, Pierson J (2007) East African megadroughts between 135 and 75 thousand years ago and bearing on early-modern human origins. Proc Natl Acad Sci 104:16416–16421

Shakun JD, Clark PU, He F, Marcott SA, Mix AC, Liu Z, Otto-Bliesner B, Schmittner A, Bard E (2012) Global warming preceded by increasing carbon dioxide concentrations during the last deglaciation. Nature 484:49–54

Siegenthaler C, Sturm M (1991) Die Häufigkeit von Ablagerungen extremer Reuss-Hochwasser. Die Sedimentationsgeschichte im Urnersee seit dem Mittelalter. In: Ursachenanalyse der Hochwasser 1987 – Ergebnisse der Untersuchungen. Mitteilungen des Bundesamtes für Wasserwirtschaft, vol 4. Bern, pp 127–139

Spakman W, Hall R (2010) Surface deformation and slab–mantle interaction during Banda arc subduction rollback. Nat Geosci 3:562–566

Stager JC, Ryves DB, Chase BM, Pausata FSR (2011) Catastrophic drought in the Afro-Asian monsoon region during Heinrich Event 1. Science 331:1299–1302

Steinke S, Mohtadi M, Prange M, Varma V, Pittauerova D, Fischer HW (2014) Mid- to Late Holocene Australian–Indonesian summer monsoon variability. Quat Sci Rev 93:142–154

Sturm M, Siegenthaler C, Pickrill RA (1995) Turbidites and 'homogenites'—a conceptual model of flood and slide deposits. In: Publication of IAS-16th regional meeting sedimentology, vol 22. Paris, p 140

Sultan N, Cochonat P, Canals M, Cattaneo A, Dennielou B, Haflidason H, Laberg JS, Long D, Mienert J, Trincardi F, Urgeles F, Vorren TO, Wilson C (2004) Triggering mechanisms of slope instability processes and sediment failures on continental margins: a geotechnical approach. Mar Geol 213:291–321

Tamuntuan G, Bijaksana S, King J, Russell J, Fauzi U, Maryunani K, Aufa N, Safiddin LO (2015) Variation of magnetic properties in sediments from Lake Towuti, Indonesia, and its paleoclimatic significance. Palaeogeogr Palaeoclimatol Palaeoecol 420:163–172

Tauhid YI, Arifian J (2000) Long-term observations on the hydrological condition of Lake Towuti. J Sains Teknol Modif Cuaca 1:93–100

Van Bemmelen RW (1970) The geology of Indonesia vol. IA: general geology of indonesia and adjacent archipelagoes, 2nd edn. Martinus Nijhoff, The Hague, p 732

Wang YJ, Cheng H, Edwards RL, An ZS, Wu JY, Shen C-C, Dorale JA (2001) A high-resolution absolute-dated Late

Pleistocene monsoon record from Hulu Cave, China. Science 294:2345–2348

Wanner H, Beer J, Bütikofer J, Crowley TJ, Cubasch U, Flückiger J, Goosse H, Grosjean M, Joos F, Kaplan JO, Küttel M, Müller SA, Prentice IC, Solomina O, Stocker TF, Tarasov P, Wagner M, Widmann M (2008) Mid- to Late Holocene climate change: an overview. Quat Sci Rev 27:1791–1828

Wicaksono SA, Russell JM, Bijaksana S (2015) Compound-specific carbon isotope records of vegetation and hydrologic change in central Sulawesi since 53,000 yr BP. Palaeogeogr Palaeoclimatol Palaeoecol 430:47–56

Wirth SB, Girardclos S, Rellstab C, Anselmetti FS (2011) The sedimentary response to a pioneer geo-engineering project: tracking the Kander River deviation in the sediments of Lake Thun (Switzerland). Sedimentology 58:1737–1761